Influence of the Dimer Interface on Glutathione Transferase Structure and Dynamics Revealed by Amide H/D Exchange Mass Spectrometry†

Simona G. Codreanu,‡ Lawrence C. Thompson,‡ David L. Hachey,‡ Heini W. Dirr,§ and Richard N. Armstrong*,‡

Departments of Chemistry and Biochemistry, Center in Molecular Toxicology, and Mass Spectrometry Research Center, Vanderbilt University School of Medicine, Nashville, Tennessee 37232-0146, and Protein Structure−Function Research Program, School of Molecular and Cell Biology, University of the Witwatersrand, Johannesburg 2050, South Africa

Received May 5, 2005; Revised Manuscript Received June 10, 2005

ABSTRACT: Mammalian glutathione (GSH) transferases are dimeric proteins, many of which share a common hydrophobic interaction motif that is important for dimer stability. In the rGSTM1-1 enzyme this motif involves the side chain of F56, located on the 56 loop of the N-terminal domain, which is intercalated between the α4- and α5-helices of the C-terminal domain of the opposing subnuit. Disruption of the complementary interactions in this motif by mutation of F56 to serine, arginine, or glutamate is known to have deleterious effects on catalytic efficiency but remarkably different effects on the stability of the dimer [Hornby et al. (2002) *Biochemistry 41*, 14238−14247]. The structural basis for the behavior of the mutants by amide H/D exchange mass spectrometry is described. A substantial decrease in H/D exchange is observed in the GSH binding domain and in parts of the dimer interface upon substrate binding. The F56S and F56R mutants exhibit enhanced H/D exchange kinetics in the GSH binding domain and at the dimer interface. In contrast, the F56E mutant shows a decrease in the rate and extent of amide H/D exchange at the dimer interface and enhanced exchange kinetics in the GSH binding domain. The results suggest that the F56E mutant has a restructured dimer interface with decreased solvent accessibility and dynamics. Although all of the F56 mutations disrupt the GSH binding site, the effects of the mutations on the structure of the subunit interface and dimer stability are quite distinct.

The canonical soluble glutathione (GSH)[1] transferases (EC 2.5.1.18) are dimeric enzymes involved in the metabolism and catabolism of xenobiotic compounds (*1*−*4*). Many GSH transferases have been well characterized both mechanistically and structurally and, as a consequence, have been used to investigate the influence of intersubunit interactions on protein stability, folding, and catalytic function (*5*−*7*). Subunit−subunit interactions at the dimer interface are known to be important for stabilizing the tertiary structure of each subunit and to enforce catalytically productive conformations at the active site. The mammalian class alpha, mu, and pi GSH transferases share a common hydrophobic interaction motif that is important for dimer stability and function (*5*−*8*). The motif in the class mu enzyme, rGSTM1-1, consists of the side chain of F56 located in the N-terminal domain of one subunit that is intercalated between helices 4 and 5 of the C-terminal domain of the opposing subunit (*9*) as illustrated in Figure 1. The F56 residue resides in a loop (hereafter referred to as the 56 loop) that is connected to the active site.

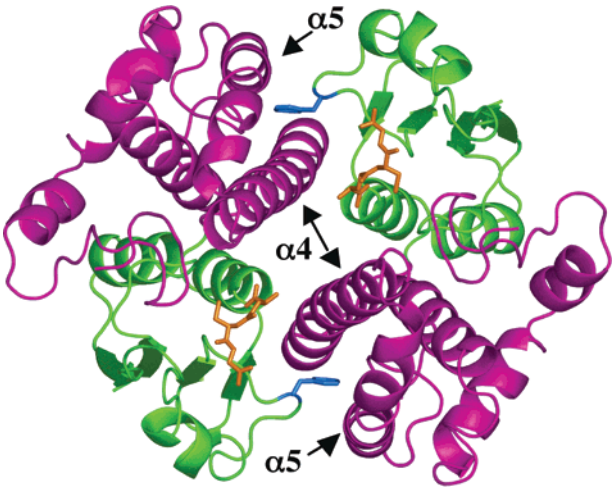

FIGURE 1: Ribbon diagram of the rGSTM1-1 dimer: N-terminal thioredoxin-like domain (green), the C-terminal α-helical domain (purple), GSH (orange), and F56 (blue). The figure was rendered with the program PyMol (*10*).

We recently demonstrated that disruption of the complementary interactions in this motif by mutation of F56 to serine, arginine, or glutamate has a deleterious effect on the catalytic efficiency but remarkably different effects on the stability of the dimer (*5*). The F56R and F56S mutations cause the equilibrium between the dimer and monomeric intermediate to shift toward the latter state while the F56E dimer is relatively more stable. The loss of catalytic

† Supported by the University of the Witwatersrand, the South African Foundation for Research and Development, Wellcome Trust Grant 060799, Forgarty International Research Collaboration Award TW00779, and Grants R01 GM30910, P30 ES00267, and T32 ES07028 from the National Institutes of Health.

* Address correspondence to this author. E-mail: r.armstrong@vanderbilt.edu. Fax: (615) 343-2921. Tel: (615) 343-2920.

‡ Vanderbilt University.

§ University of the Witwatersrand.

[1] Abbreviations: GST, glutathione transferase; CDNB, 1-chloro-2,4-dinitrobenzene; DTNB, dithiobis(2-nitrobenzoic acid); DTT, dithiothreitol; EDTA, ethylenediaaminetetraacetic acid; GSH, reduced glutathione; GSO_3^-, glutathionesulfonate; IPTG, isopropyl thioglucopyranoside; MOPS, 3-(*N*-morpholino)propanesulfonic acid; PCR, polymerase chain reaction.

10.1021/bi050836k CCC: $30.25
Published on Web 07/16/2005

efficiency of the mutants is not related to dissociation of the dimer but rather to a structural disruption of the glutathione binding site that is coupled to the dimer interface through the 56 loop. The mutant proteins have proven difficult to crystallize so that the structural bases for the loss of catalytic function and dimer stability have remained an enigma.

In this paper we report the use of amide H/D exchange mass spectrometry to probe the alterations in the solvent accessibility of the protein in response to substrate (GSH) binding and to the alteration of the dimer interface. A substantial decrease in H/D exchange is observed in the GSH binding domain and in parts of the dimer interface upon substrate binding. Both the F56S and F56R mutants exhibit enhanced H/D exchange kinetics in the GSH binding domain and at the dimer interface. In contrast, the F56E mutant shows a decrease in the rate and extent of amide H/D exchange at the dimer interface and enhanced exchange kinetics in the GSH binding domain. The results suggest that the F56E mutant has a restructured dimer interface with decreased solvent accessibility and dynamics. All of the F56 mutations disrupt the GSH binding site, demonstrating a delicate interplay between the dimer interface structure and catalysis.

EXPERIMENTAL PROCEDURES

Materials. Deuterium oxide (99.9 atom % D), pepsin, glutathione, glutathionesulfonate (GSO_3^-), and protease inhibitor cocktail were purchased from Sigma (St. Louis, MO). Trifluoroacetic acid (peptide synthesis grade) was purchased from Pierce Chemicals (Rockford, IL). Acetonitrile (HPLC grade) was purchased from EM Science (Gibbstown, NJ). Anhydrous monobasic potassium phosphate was purchased from Fisher Scientific (Pittsburgh, PA). The pET20b-(+) expression vector, the *Escherichia coli* strains BL21-(DE3) and DH5α, the restriction enzymes *Nde*I, *Hin*dIII, *Xba*I, *Stu*I, *Bgl*I, *and Sac*II, and benzonase were purchased from Novagen (Madison, WI). All other chemical reagents were purchased from commercial sources and were used without further purification. All of the solutions were prepared and used on the same day. GSH concentrations were confirmed by titration with DTNB (*11*).

Preparation of Native and Mutant Proteins. The expression vectors for the dimer interface mutants were generated by site-specific mutagenesis as previously described (*5*). The native and mutant enzymes were overexpressed in *E. coli* strain BL21(DE3), and cells were grown in LB medium containing ampicillin (100 μg/mL). The cell culture was grown at 37 °C with vigorous shaking until the OD_{600} = 1.0. Cells were induced with IPTG for 3 h (0.7 mM final concentration). Cells were then harvested by centrifugation (6500*g*, 15 min, 4 °C) and pellets resuspended in 50 mM Tris buffer containing 1 mM EDTA and 1 mM DTT (pH 7.5). Cells were lysed by sonication and treated with 1 mL of 10× protease inhibitor cocktail solution, and cell debris was removed by centrifugation (35000*g*, 35 min, 4 °C). The supernatant was then treated with benzonase for 2 h at room temperature to digest nucleic acids and then dialyzed against 20 mM MOPS buffer containing 1 mM EDTA and 1 mM DTT (pH 6.8). The proteins were applied to a cationic exchange SP-Sepharose column (2 × 15 cm), previously equilibrated with the same buffer and eluted with a linear salt gradient (0−500 mM NaCl) in the same buffer. Fractions containing protein were pooled together and dialyzed against 20 mM KH_2PO_4 buffer containing 1 mM EDTA and 1 mM DTT (pH 6.8). The protein solutions were further applied to a hydroxyapatite column (2 × 10 cm), previously equilibrated with the phosphate buffer, and eluted with gradient buffer (20−400 mM KH_2PO_4) containing 1 mM EDTA and 1 mM DTT (pH 6.8).

For the mass spectrometry experiments, which require very high protein purity, all native and mutant enzymes were subsequently applied to a cationic exchange Mono-S HR 5/5 column, previously equilibrated with 5 mM KH_2PO_4 buffer (pH 7.0). The proteins were eluted at a flow of 1 mL/min with a 20 min linear salt gradient (0−500 mM NaCl) prepared in the same buffer. Fractions containing purified protein were combined, dialyzed against 20 mM KH_2PO_4 buffer containing 1 mM EDTA and 1 mM DTT (pH 7.0), concentrated, flash-frozen, and stored at −80 °C. The purity of the proteins was assessed by SDS−PAGE, and their identity was confirmed by MALDI-MS. Protein concentrations for the monomeric species of native and F56E, F56R, and F56S mutant enzymes were determined spectrophotometrically using a molar extinction coefficient of 40060 M^{-1} cm^{-1} at 280 nm (*12*).

Sample Preparation for H/D Exchange Experiments. Protein samples for the H/D exchange experiments were dialyzed against 0.1 M potassium phosphate buffer (pH 6.9) overnight and were filtered prior to use through a 0.2 μm filter to remove particulate matter and any insoluble protein. A stock solution of 500 μM (13 mg/mL) was flash-frozen and stored at −80 °C in small aliquots. Each aliquot was sufficient for 20 deuterium exchange mass spectrometric analyses and was used within 1 day of thawing.

Hydrogen/Deuterium Exchange. Hydrogen/deuterium exchange experiments for the free native or mutant enzymes were designed similarly to those reported previously (*13*). Deuterium exchange was initiated by diluting 10 μL of the equilibrated protein solution (13 mg/mL) 10-fold with 90 μL of D_2O. The protein/D_2O solution was incubated at 24 °C for various times (from 10 s to 6 h). At each time point, the reaction was quenched by cooling (tubes transferred to an ice bath) and acidified by adding 100 μL of quench buffer [0.1 M potassium phosphate buffer (pH 2.4) in H_2O at 0 °C]. After 30 s, 10 μL of pepsin (12 mg/mL in H_2O at 0 °C) was added to the quenched sample, and the resultant sample was incubated on ice for 5 min. All of the samples for one protein (16 time points) were prepared individually and run on the same day.

The following changes were used to study the H/D exchange of the native enzyme or the F56S mutant with ligand bound. At the start of the day, concentrated protein stocks were mixed with GSH or GSO_3^- (ligand solutions prepared in 0.1 M potassium phosphate buffer, pH 7.0) to a final concentration of 600 μM protein and 2 mM GSH (native), 1.5 mM GSO_3^- (native), or 200 mM GSO_3^- (F56S). The addition of D_2O results in a final concentration of 60 μM protein and 200 μM GSH, 150 μM GSO_3^-, or 20 mM GSO_3^-, respectively. Final ligand concentrations are equal to $5K_m$ for native + GSH and $5K_i$ for native or F56S + GSO_3^- (*5*, *14*). The protein/ligand/D_2O solution was incubated at 25 °C for various times (from 15 s to 8.5 h) to generate a total of 12 time points.

Electrospray Ionization Mass Spectrometry. The extent of deuterium incorporation into the peptide fragments was determined by LC/MS using the same protocol described previously (*13*). Mass determinations for the free proteins were performed using a Finnigan MAT TSQ-7000 triple quadrupole mass spectrometer (Finnigan Corp., San Jose, CA) and for the ligand-bound proteins using a Finnigan TSQ quantum triple quadrupole mass spectrometer (Finnigan Corp., San Jose, CA), both equipped with a standard electrospray ionization source outfitted with a 100 μm i.d. deactivated fused silica capillary. The mass spectrometer was operated in full scan mode using Quad 1. The analyzer was calibrated and tuned to unit resolution with a peak width at half-height of 0.7. The data were collected from *m*/*z* 300 to *m*/*z* 900 with a 1 s scan time.

Data acquisition and spectral analysis were conducted using Finnigan Xcalibur software (version 1.3) on a Dell Optiplex GX270 computer running the Microsoft Windows 2000 operating system. The centroid data were analyzed using MagTran 1.0 beta9 software written by Zhang and Marshall (*15*).

Kinetic Analysis. The amount of deuterium incorporated in each peptide was adjusted for back-exchange as described previously (*13*) and plotted versus time. Two data sets were averaged for each experiment. Progress curves for individual peptides were fitted to the sum of first-order rate terms according to eq 1, using the program Prism 4.0 (Graphpad Software), where D is the deuterium content of a peptide, N is the number of peptide amide protons, k_i is the exchange rate constant for each amide hydrogen, and t is the time allowed for isotope exchange (*16*).

$$D = N\sum_{i=1}^{N}\exp(-k_i t) \quad (1)$$

The total number of exponential terms chosen was based on the goodness of each fit. The minimum number terms were used to get the best fit and smallest error. The kinetic data are tabulated as amplitudes A_1 (D), A_2 (D), ..., A_i (D) and the associated rate constants k_1, k_2, ..., k_i for each exponential. The errors are obtained from the least-squares fit of the data to the appropriate exponential equation.

Computer-Generated Model of the F56E Mutant. A model of the F56E mutant was generated with the mutation protocol in the program Insight II (*17*). This protocol changes the side chain to the appropriate amino acid without altering the protein backbone and chooses the best rotamer of the new side chain. Other side-chain rotamers were checked manually to confirm that the selected conformation was the only one without significant van der Waals clashes.

RESULTS

Amide H/D Exchange Kinetics of the Native Enzyme. Rapidly exchangeable backbone amides ($k_x > 4$ min^{-1}) are the best predictors of solvent accessibility and protein secondary structure (*18*−*20*). Figure 2A illustrates the extent of exchange in the rapid kinetic phase for the native enzyme. The N-terminal thioredoxin-like domain shows a modest amount (15−30%) of fast exchange in the absence of substrate. Solvent exclusion is much more apparent in the α-helical domain beginning with the α4-helix and extending through the core of the molecule through the α8-helix. The

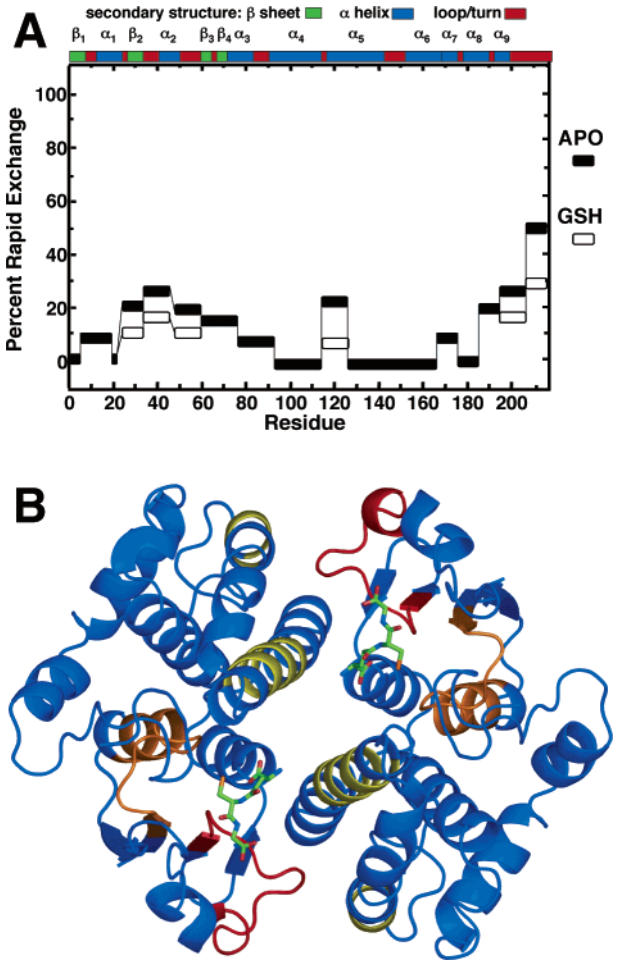

FIGURE 2: Panel A shows the H/D exchange profile of rapidly exchanging amides (those that are exchanged within 15 s) first across the native M1-1 sequence in both apo (solid bars) and ligand-bound forms (open bars). Ligand-bound enzyme showed similar exchange profiles except where noted. Panel B is a ribbon diagram of the rGSTM1-1 backbone (blue) showing peptides that probe vital regions of the structure including residues 5−20 in the active site (orange), residues 49−62 in the F56 loop (red), and residues 101−110 of α4 and 137−140 of α5 in the hydrophobic pocket (yellow).

first two helices (α4 and α5) of this domain show no rapidly exchanging amides while the loop that connects them (peptide 114−126) is 30% exchanged after 15 s. Solvent exclusion from these helices is consistent with the tight dimer interface packing seen in the crystal structure (*9*). The last 30 residues of the enzyme show a gradual increase in solvent accessibility. The C-terminal tail, peptide 209−217, is the most solvent exposed with 50% of its amides exchanging in the first 15 s. The last helix (α9) and the C-terminal tail are on the surface of the protein and would be expected to exchange rapidly.

There are three peptides in the native enzyme that show no exchange over the 8.5 h length of the experiment. These are peptides 19−21, 92−100, and 158−163. Peptide 92−100 is contained in α4 and, as mentioned above, is tightly packed against the opposing monomer. It is also in close contact with α5. Peptide 158−163 is located in the core of a helical bundle involving α4, α5, and α6. This bundle is believed to be responsible for the overall stability of the C-terminal domain. The lack of exchange in this region is consistent with that hypothesis. Peptide 19−21 is located in the center of α1, which is sandwiched between the β-sheet of

Table 1: Rate Constants (k) and Amplitudes (A) for Main-Chain Amide H/D Exchange into Peptides 7−20 and 8−20 in the Presence of GSH or GSO_3^- [a]

peptide/ligand	A_1 (D)	k_1 (min^{-1})	A_2 (D)	k_2 (min^{-1})	A_3 (D)	k_3 (min^{-1})
7−20/GSH	0.86 ± 0.05	0.27 ± 0.04	3.6 ± 0.1	0.013 ± 0.002	7.0 ± 0.1	$(1.8 \pm 0.3) \times 10^{-4}$
8−20/GSH	0.85 ± 0.07	0.25 ± 0.04	3.1 ± 0.1	0.013 ± 0.001	6.6 ± 0.2	$(8 \pm 5) \times 10^{-5}$
(7−20)−(8−20)[b]	0.84 ± 0.02	$(7.0 \pm 0.6) \times 10^{-3}$				
7−20/GSO_3^-	1.26 ± 0.09	0.5 ± 0.1	2.8 ± 0.5	0.01 ± 0.002	7.9 ± 0.5	$(3 \pm 1) \times 10^{-4}$
8−20/GSO_3^-	1.19 ± 0.06	0.50 ± 0.06	2.8 ± 0.5	0.008 ± 0.001	6.9 ± 0.5	$(1 \pm 1) \times 10^{-4}$
(7−20)−(8−20)[b]	0.92 ± 0.02	$(5.1 \pm 0.6) \times 10^{-3}$				

[a] The errors in the amplitudes and rate constants are from fits of the experimental data to the appropriate exponential expression. [b] Difference kinetics isolating the main-chain amide of N8 in the presence of GSH and GSO_3^-.

the N-terminal domain and α5 of the C-terminal domain (*9*).

The peptic digest also gave four peptides that are good probes of the local dynamics in that active site and the dimer interface (Figure 2B). Peptide 5−20 (including 5−18, 7−18, 7−20, and 8−20) probes the active site and contains residues Y6 and W7 that contribute the binding of GSH. Peptide 49−62 covers the entire loop region including F56. Peptides 101−100 and 137−140 cover the majority of the hydrophobic binding pocket.

Amide H/D Exchange Kinetics of the Native Enzyme with Ligand Bound. Backbone amide H/D exchange experiments were performed in the presence of 200 μM GSH or 150 μM GSO_3^-. The enzyme−GSH complex exhibits decreases in H/D exchange in several regions of the protein. These are best illustrated by the rapidly exchangeable amides (Figure 2). The decreases in the exchange kinetics are observed in but not confined to the GSH binding site. Interestingly, there is a marked reduction in the extent of rapid exchange at the turn between the α4- and α5-helices (peptide 114−126) and the C-terminal tail including the α9-helix. These structural elements define the channel for the approach to the active site (*9*).

The kinetic profiles for H/D exchange of native enzyme in the presence of either GSH or the substrate analogue GSO_3^- are identical except for four peptides (5−18, 7−18, 7−20, and 8−20) at the active site (Figure 3). The enzyme−GSO_3^- complex exhibits small but reproducible changes in the amplitudes and rate constants for exchange of amides in the intermediate and slow time regime ($k_x < 4$ min^{-1}). Although the overall changes are small, all four peptides across this region show similar behavior. The spatial resolution can be increased by subtraction of the kinetic data from two overlapping peptides as illustrated in Figure 3 for the backbone N−H of N8. The side chains of the two preceding residues, W7 and Y6, contribute hydrogen-bonding interactions with the cysteinyl carbonyl oxygen and the sulfur of GSH, respectively (*9*). The H/D exchange kinetics are sufficiently sensitive to detect the difference between a thiolate anion and sulfonate group in the active site.[2]

Amide H/D Exchange Kinetics of the Dimer Interface Mutants. Not surprisingly, the impact of mutations on the H/D exchange kinetics is greatest at the site of mutation (peptide 49−62) and in the hydrophobic binding pocket (peptides 101−110 and 137−140). Significant changes also extend into the GSH binding site (peptide 5−18). However, the effect of the mutation differs markedly with the charge of the side chain.

[2] A similar observation has also been made in the unrelated microsomal GSH transferase MGST1 (L. S. Busenlehner and R. N. Armstrong, unpublished results).

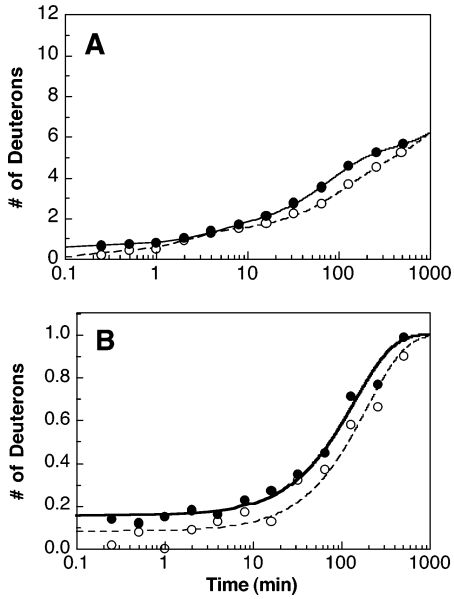

FIGURE 3: (A) H/D exchange profile of peptide 7−20 in the presence of 200 μM GSH (●) or 150 μM GSO_3^- (○). (B) Difference H/D exchange profile (peptide 7−20 minus peptide 8−20) in the presence of 200 μM GSH (●) or 150 μM GSO_3^- (○). The lines are fits of the data to exponentials with the amplitudes and rate constants given in Table 1.

The F56R and F56S mutants show increases in the fraction of rapidly exchanging amides in the loop harboring the mutation, a fact that is indicative of a higher degree of solvent access or increased loop dynamics (Figure 4A). In sharp contrast, the F56E mutant exhibits a marked decrease in the extent of rapid exchange. The F56S mutant retains the ability to bind the substrate analogue inhibitor GSO_3^- ($K_i = 4$ mM) (*5*), and the addition of ligand (GSO_3^-) to the F56S mutant tends to restore the nativelike H/D exchange kinetic profile as shown in Figure 4B.

Like the loop that harbors F56, the helices that define the hydrophobic pocket in both the F56R and F56S mutants exhibit increases in H/D exchange rates relative to the native enzyme (Figure 5A,C). However, the increases observed are in the intermediate and slow phase regimes of the exchange kinetics. This suggests that the α4/α5 helices have not been perturbed structurally but that the dynamics of this region have been increased. Addition of ligand to the F56S mutant also produces a reduction in exchange kinetics when compared to the apoenzyme. However, the rescue of nativelike behavior is not complete particularly with respect to the α5-helix, peptide 137−140 (Figure 5B,D). The F56S mutant still shows enhanced exchange kinetics in the slow phase regime. Thus, binding of GSO_3^- does not completely restore the native structure or dynamics of this region.

Table 2: Rate Constants and Amplitudes for Main-Chain Amide H/D Exchange into the F56 Loop at the Dimer Interface (Peptide 49−62)[a]

sample	A_1 (D)	k_1 (min^{-1})	A_2 (D)	k_2 (min^{-1})	A_3 (D)	k_3 (min^{-1})
native	3.6 ± 0.2	0.7 ± 0.1	2.5 ± 0.1	(2 ± 2) × 10−4		
F56R	0.8 ± 0.1	0.3 ± 0.1	2.2 ± 0.1	(3.2 ± 0.3) × 10^{-3}		
F56E	5.9 ± 0.2	0.32 ± 0.03	1.8 ± 0.2	(5 ± 1) × 10^{-3}		
F56S	1.7 ± 0.1	0.24 ± 0.05				
native/GSO_3^-	4.7 ± 0.5	0.7 ± 0.2	1.4 ± 0.4	0.024 ± 0.016		
F56S/GSO_3^-	5.4 ± 0.3	2.4 ± 0.2	1.4 ± 0.1	0.04 ± 0.01	3.8 ± 0.1	(6 ± 1) × 10^{-4}

[a] The errors in the amplitudes and rate constants are from fits of the experimental data to the appropriate exponential expression.

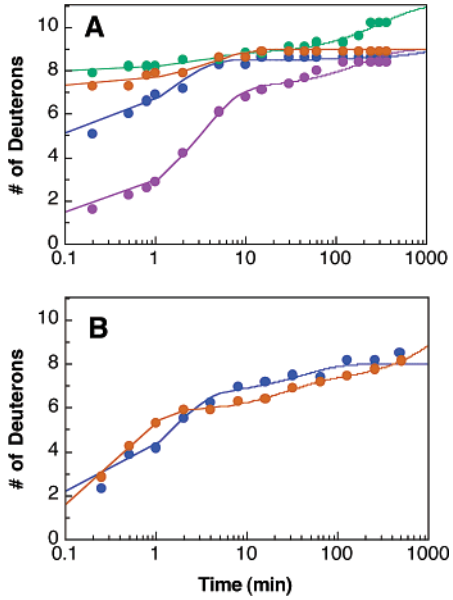

FIGURE 4: Kinetic profiles for H/D exchange of backbone amides at the site of mutation, peptide 49−62. Panel A illustrates the kinetic profiles for the apo proteins including the native enzyme (blue), F56S (orange), F56R (green), and F56E (magenta). Panel B shows the kinetic profiles for the native enzyme (blue) in the presence of 150 μM GSO_3^- and the F56S mutant (orange) in the presence of 20 mM GSO_3^-. The solid lines are fits of the data to multiple exponentials with the rate constants and amplitudes given in Table 2.

The F56E mutant shows a significant decrease in rate of H/D exchange particularly in the α4-helix (peptide 101−110) but relatively small differences in the α5-helix (peptide 137−140) (Figure 5A,C) when compared to the native enzyme. This result, together with the reduced rates of exchange in the 56 loop noted above, suggests that the dimer interface adopts a new and less solvent accessible conformation in this mutant. The mutations at the dimer interface also influence the amide H/D exchange behavior in the GSH binding site as illustrated in Figure 6 for peptide 5−18. Both the F56R and F56E mutants exhibit significant increases in the extent of exchange in the fast phase kinetic regime. In contrast, the F56S mutant exhibits more nativelike exchange behavior in this region. All of the mutants have large increases in the K_m for GSH and K_i for GSO_3^- (*5*), which indicates that the mutations introduce a functional disruption of the active site. The insertion of a charged side chain into the hydrophobic pocket at the subunit interface (F56R and F56E) results in the most significant functional impairment and more dramatic changes in the H/D exchange kinetic profiles consistent with a more disordered or solvent-accessible GSH binding site. Though the F56S mutant is also functionally impaired, the H/D exchange kinetics are much more nativelike. In fact, with the addition of GSO_3^- (Figure 6B), the native and F56S mutants are almost indistinguishable in their exchange profiles.

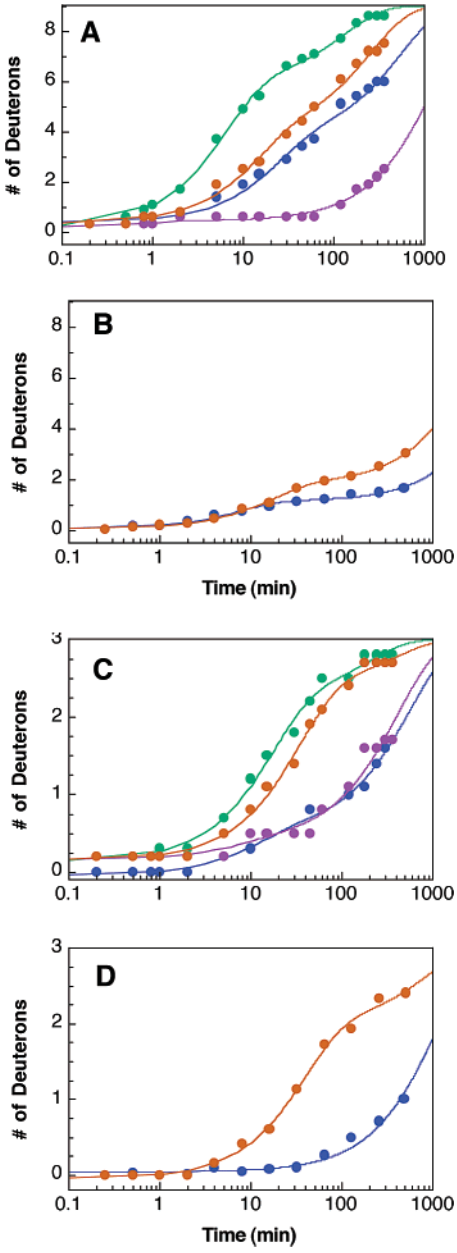

FIGURE 5: Kinetic profiles for H/D exchange of main-chain amides surrounding the hydrophobic pocket formed by α4 (peptide 101−110) in panels A and B and α5 (peptide 137−140) in panels C and D. Panels A and C illustrate the kinetic profiles for apoenzymes, including native (blue), F56 (orange), F56R (green), and F56E (magenta). Panels B (peptide 101−110) and D (peptide 137−140) illustrate the exchange profile for the native enzyme in the presence of 150 μM GSO_3^- (blue) and the F56S mutant in the presence of 20 mM GSO_3^- (orange). The solid lines are fits of the data to multiple exponentials with the rate constants and amplitudes given in Table 3.

Table 3: Rate Constants and Amplitudes for Main-Chain Amide H/D Exchange near the Hydrophobic Pocket between the α4- and α5-Helices at the Dimer Interface (Peptides 101−110 and 137−140)[a]

peptide/sample	A_1 (D)	k_1 (min^{-1})	A_2 (D)	k_2 (min^{-1})
101−110 native	3.3 ± 0.4	0.04 ± 0.01	5.3 ± 0.4	(1.9 ± 0.3) × 10^{-4}
101−110 F56R	5.7 ± 0.2	0.16 ± 0.01	3.1 ± 0.2	(7.7 ± 0.8) × 10^{-4}
101−110 F56E	0.24 ± 0.18	1.1 ± 1.5	8.6 ± 0.1	(7.6 ± 0.4) × 10^{-4}
101−110 F56S	3.6 ± 0.3	0.07 ± 0.01	5.1 ± 0.3	(3.9 ± 0.4) × 10^{-3}
101−110 native/GSO_3^-	1.4 ± 0.1	0.09 ± 0.01	7.7 ± 0.1	(1.5 ± 0.2) × 10^{-3}
101−110 F56S/GSO_3^-	1.1 ± 0.1	0.13 ± 0.02	7.85 ± 0.05	(1.5 ± 0.3) × 10^{-4}
137−140 native	0.6 ± 0.1	0.08 ± 0.02	2.5 ± 0.1	(1.8 ± 0.1) × 10^{-3}
137−140 F56R	2.1 ± 0.2	0.06 ± 0.01	0.8 ± 0.2	(5 ± 2) × 10^{-3}
137−140 F56E	0.2 ± 0.1	0.12 ± 0.16	2.6 ± 0.1	(2.4 ± 0.3) × 10^{-3}
137−140 F56S	2.2 ± 0.2	0.030 ± 0.004	0.6 ± 0.2	(2.6 ± 1.3) × 10^{-3}
137−140 native/ GSO_3^-	2.96 ± 0.02	(9.0 ± 0.6) × 10^{-4}		
137−140 F56S/GSO_3^-	2.0 ± 0.1	0.026 ± 0.003	1.0 ± 0.1	(1.2 ± 0.4) × 10^{-3}

[a] The errors in the amplitudes and rate constants are from fits of the experimental data to the appropriate exponential expression.

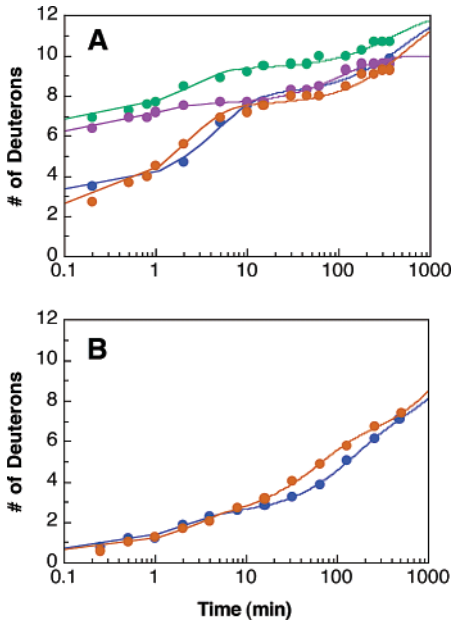

FIGURE 6: Kinetic profiles for H/D exchange of peptide 5−18 at the GSH binding site. Panel A shows exchange profiles for the apoenzymes: native (blue), F56S (orange), F56R (green), and F56E (magenta). Panel B shows exchange profiles of the native enzyme in the presence of 150 μM GSO_3^- (blue) and the F56S mutant in the presence of 20 mM GSO_3^- (orange). The solid lines are fits of the experimental data to multiple exponentials with rate constants and amplitudes given in Table 4.

DISCUSSION

Substrate Binding and the Dimer Interface. Previous functional studies have suggested that there is close link between the structure of the dimer interface and the GSH binding site (*5*). This link is apparent in the influence of GSH binding on the amide H/D exchange kinetics. In addition to the reduction in exchange rates at the GSH binding site, there are notable decreases at the dimer interface including the loop harboring F56, the junction between the α4 and α5-helices, and more remotely at the C-terminal tail as illustrated in Figure 7. These results are consistent with previous observations of decreased amide H/D exchange by NMR spectroscopy in the human class mu enzyme upon ligand binding at the active site (*20*). The reduced rates of exchange at the subunit interface and the C-terminal tail that do not directly interact with GSH are likely due to a damping of low-frequency (> 10^{-6} s) conformational excursions that lead to increased solvent exposure of the backbone. In this regard it is important to point out that the side chain of P60 and the base of the 56 loop are in van der Waals contact with Y6, a residue that directly interacts with the sulfur of GSH.

The substrate analogue inhibitor, GSO_3^-, has essentially the same effect on the H/D exchange kinetics of the native enzyme with the exception of subtle changes that occur in peptides located close to the thiolate or sulfonate groups. The 30% reduction in the rate constant for H/D exchange at N8 in the E·GSO_3^- complex compared to the E·GS^- complex (Figure 3, Table 1) suggests that GSO_3^- forms a tighter complex that more effectively limits conformational fluctuations at the active site. This observation is also consistent with the fact that GSO_3^- has a lower off rate than GS^- (*14*).

Structure and Dynamics of the Dimer Interface Mutants. "Ball and socket" hydrophobic interactions are common stabilizing motifs in oligomeric protein structures (*21*). The mutational disruption of this type of interaction in the class mu GSH transferase has been previously demonstrated to alter dimer stability and impair the catalytic function of the mutants (*5*). The loss of catalytic function is associated with a disruption of the structure of the GSH binding site. Inasmuch as the predominant form of the enzyme in the exchange experiments is the dimer [all enzymes at 60 μM (*5*) during exchange (see Experimental Procedures)], the changes in H/D exchange kinetics exhibited by the mutant enzymes provide new insight into the structural bases for the altered behavior. The F56S and F56R mutants show enhanced exchange at the dimer interface as well as in the active site, indicating that the mutations result in larger coupled conformational excursions in these regions. The enhanced exchange, which is more apparent in the F56R mutant (Figure 8A), correlates with the lower dimer stability and catalytic activity of this mutant.

The changes in the amide H/D exchange kinetics associated with the more benign F56S mutation are most apparent in the α5-helix (peptide 137−140) and are not reversed when the GSH binding site is occupied with the inhibitor GSO_3^- (Figure 5C,D). Thus it is not clear that the conformation of the GSH binding site is completely coupled to the conformational integrity of the dimer interface. Residues Y137 and F140 form part of the hydrophobic socket located between the α4- and α5-helices. It could be the case that the dynamics of the dimer interface in the F56S mutant are similar to those of the native enzyme. The small hydrophilic side chain of

Table 4: Rate Constants and Amplitudes for Main-Chain Amide H/D Exchange near the GSH Binding Site, Peptide 5−18[a]

sample	A_1 (D)	k_1 (min^{-1})	A_2 (D)	k_2 (min^{-1})	A_3 (D)	k_3 (min^{-1})
native	4.7 ± 0.2	0.21 ± 0.03	3.9 ± 0.1	(1.9 ± 0.2) × 10^{-3}		
F56R	2.6 ± 0.2	0.46 ± 0.08	2.6 ± 0.1	(2.4 ± 0.3) × 10^{-3}		
F56E	1.4 ± 0.3	1.2 ± 0.4	2.4 ± 0.1	(8.5 ± 0.8) × 10^{-3}		
F56S	5.1 ± 0.2	0.47 ± 0.06	4.5 ± 0.1	(1.8 ± 0.2) × 10^{-3}		
native/GSO_3^-	1.7 ± 0.2	0.5 ± 0.1	3.7 ± 1.5	0.007 ± 0.003	5.9 ± 1.6	(4 ± 4) × 10^{-4}
F56S/GSO_3^-	1.7 ± 0.2	0.4 ± 0.1	3.6 ± 0.3	0.017 ± 0.004	6.1 ± 0.4	(6 ± 2) × 10^{-4}

[a] The errors in the amplitudes and rate constants are from fits of the experimental data to the appropriate exponential expression.

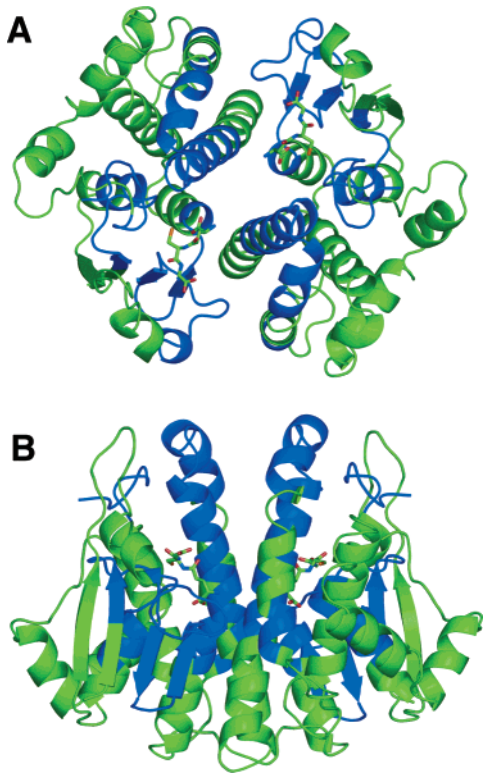

FIGURE 7: Decreases (blue) in H/D exchange kinetics in the native + GSH versus the apoenzyme (A) viewed down the 2-fold axis of the dimer and (B) perpendicular to the 2-fold axis. The GSH molecule and Y6 are shown in stick representation. The figure was rendered with the program PyMol (*10*).

S56 may simply facilitate entry of solvent (and hydroxide ion) into the socket and therefore enhance exchange in peptide 137−140.

Perhaps the most interesting mutant is F56E. The introduction of the glutamate side chain at position 56 results in dramatic decreases in the H/D exchange rates in the F56 loop and the α4-helix and much smaller changes in the α5-helix at the dimer interface as illustrated in Figure 8B. This result suggests that this particular mutation, in contrast to the others, causes a diminution in solvent access at the interface probably due to the adoption of an alternative conformation that is less prone to low-frequency excursions. The exact structure of this new conformation is not known. However, modeling of a glutamate side chain into the native structure (Figure 8C) places the carboxyl of E56 about 3.5 Å from the carboxamide of Q102 on the α4-helix. So, it is possible that a hydrogen-bonding interaction between the side chains of E56 and Q102 could develop after some adjustment in the conformation of the loop and the α4-helix. Inasmuch as the immediate environment of the socket is largely hydrophobic, this interaction could be quite substantial and

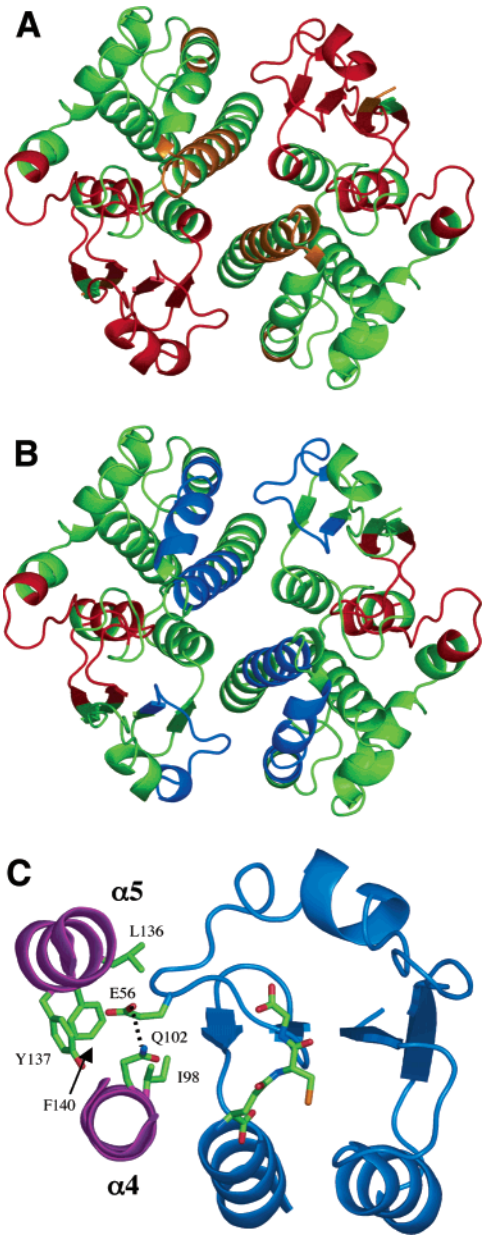

FIGURE 8: Changes in the amide H/D exchange kinetics in (A) the F56R mutant and (B) the F56E mutant compared to the native enzyme in the absence of ligands. Regions with decreases in rates of exchange are shown in blue while increases in exchange in the rapid phase and intermediate/slow phases are shown in red and orange, respectively. (C) The computer-generated (see Experimental Procedures) structure of the F56E mutation indicates the possibility of hydrogen-bonding interactions with Q102 (3.45 Å). GSH is shown as a stick with important side chains noted. The figure was rendered with the program PyMol (*10*).

could explain why the dimer of the F56E mutant is at least as stable as the native enzyme (*5*).

Additional evidence that the 56 loop adopts an alternative conformation in the F56E mutant is the disruption of the GSH binding site and the enhanced H/D exchange in the active site (Figure 8B). Of the three mutants F56E is the most seriously compromised with respect to catalytic function (*5*). It appears that the altered and apparently less flexible conformation at the dimer interface is transmitted into the GSH binding site.

Conclusions. Main-chain amide H/D exchange kinetics provides a direct readout of the effect of mutations on the structure and dynamics on the dimer interface of rGSTM1-1 and the remote influence on enzyme function. Disruption of the hydrophobic ball and socket motif leads to an impairment of catalytic function irrespective of whether dimer stability or protein dynamics at the subunit interface are increased or decreased.

SUPPORTING INFORMATION AVAILABLE

Tables S1 and S2 containing a complete set of the rate constants and amplitudes used to fit kinetic profiles for all peptides and Figures S1−S36 describing the kinetic profiles for H/D exchange for all peptides. This material is available free of charge via the Internet at http://pubs.acs.org.

REFERENCES

1. Armstrong, R. N. (1997) Structure, catalytic mechanism, and evolution of the glutathione transferases, *Chem. Res. Toxicol. 10*, 2−18.
2. Edwards, R., Dixon, D. P., and Walbot, V. (2000) Plant glutathione S-transferases: enzymes with multiple functions in sickness and in health, *Trends Plant Sci. 5*, 193−198.
3. Sheehan, D., Meade, G., Foley, V. M., and Dowd, C. A. (2001) Structure, function and evolution of glutathione transferases: implications for classification of non-mammalian members of an ancient enzyme superfamily, *Biochem. J. 360*, 1−16.
4. Josephy, P. (1997) *Molecular Toxicology*, Oxford University Press, Oxford.
5. Hornby, J. A., Codreanu, S. G., Armstrong, R. N., and Dirr, H. W. (2002) Molecular recognition at the dimer interface of a class mu glutathione transferase: role of a hydrophobic interaction motif in dimer stability and protein function, *Biochemistry 41*, 14238−14247.
6. Stenberg, G., Abdalla, A. M., and Mannervik, B. (2000) Tyrosine 50 at the subunit interface of dimeric human glutathione transferase P1-1 is a structural key residue for modulating protein stability and catalytic function, *Biochem. Biophys. Res. Commun. 271*, 59−63.
7. Sayed, Y., Wallace, L. A., and Dirr, H. W. (2000) The hydrophobic lock-and-key intersubunit motif of glutathione transferase A1-1: implications for catalysis, ligandin function and stability, *FEBS Lett. 465*, 169−172.
8. Dirr, H., Reinemer, P., and Huber, R. (1994) X-ray crystal structures of cytosolic glutathione S-transferases. Implications for protein architecture, substrate recognition and catalytic function, *Eur. J. Biochem. 220*, 645−661.
9. Ji, X., Zhang, P., Armstrong, R. N., and Gilliland, G. L. (1992) The three-dimensional structure of a glutathione S-transferase from the mu gene class. Structural analysis of the binary complex of isoenzyme 3-3 and glutathione at 2.2-Å resolution, *Biochemistry 31*, 10169−10184.
10. Delano, W. L. PyMol [The PyMOL Molecular Graphics System (http://www.pymol.org)].
11. Ellman, G. L. (1959) Tissue sulfhydryl groups, *Arch. Biochem. Biophys. 82*, 70−77.
12. Edelhoch, H. (1967) Spectroscopic determination of tryptophan and tyrosine in proteins, *Biochemistry 6*, 1948−1954.
13. Codreanu, S. G., Ladner, J. E., Xiao, G., Stourman, N. V., Hachey, D. L., Gilliland, G. L., and Armstrong, R. N. (2002) Local protein dynamics and catalysis: detection of segmental motion associated with rate-limiting product release by a glutathione transferase, *Biochemistry 41*, 15161−15172.
14. Parsons, J. F., Xiao, G., Gilliland, G. L., and Armstrong, R. N. (1998) Enzymes harboring unnatural amino acids: mechanistic and structural analysis of the enhanced catalytic activity of a glutathione transferase containing 5-fluorotryptophan, *Biochemistry 37*, 6286−6294.
15. Zhang, Z., and Marshall, A. G. (1998) A universal algorithm for fast and automated charge state deconvolution of electrospray mass-to-charge ratio spectra, *J. Am. Soc. Mass Spectrom. 9*, 225−233.
16. Zhang, Z., Post, C. B., and Smith, D. L. (1996) Amide hydrogen exchange determined by mass spectrometry: application to rabbit muscle aldolase, *Biochemistry 35*, 779−791.
17. Accelrys Insight II (http://www.accelrys.com/products/insight/).
18. Resing, K. A., Hoofnagle, A. N., and Ahn, N. G. (1999) Modeling deuterium exchange behavior of ERK2 using pepsin mapping to probe secondary structure, *J. Am. Soc. Mass Spectrom. 10*, 685−702.
19. Hoofnagle, A. N., Resing, K. A., and Ahn, N. G. (2003) Protein analysis by hydrogen exchange mass spectrometry, *Annu. Rev. Biophys. Biomol. Struct. 32*, 1−25.
20. Bai, Y., Milne, J. S., Mayne, L., and Englander, S. W. (1993) Primary structure effects on peptide group hydrogen exchange, *Proteins 17*, 75−86.
21. Jones, S., and Thornton, J. M. (1995) Protein-protein interactions: a review of protein dimer structures, *Prog. Biophys. Mol. Biol. 63*, 31−65.

BI050836K